Electrogyration in metamaterials: Chirality and polarization rotatory power that depend on applied electric field

Qiang Zhang, Eric Plum, Jun-Yu Ou, Hailong Pi, Junqing Li,* Kevin F. MacDonald,* and Nikolay I. Zheludev**

Qiang Zhang, Dr. Eric Plum, Dr. Jun-Yu Ou, Prof. Kevin F. MacDonald, and Prof. Nikolay I. Zheludev
Optoelectronics Research Centre and Centre for Photonic Metamaterials, University of Southampton, Southampton, SO17 1BJ, United Kingdom
E-mail: erp@orc.soton.ac.uk, kfm@orc.soton.ac.uk, niz@orc.soton.ac.uk

Qiang Zhang, Prof. Junqing Li
School of Physics, Harbin Institute of Technology, 92 Western Dazhi, Harbin 150001, China
E-mail: jqli@hit.edu.cn

Hailong Pi
School of Electronics and Computer Science, University of Southampton, Southampton, SO17 1BJ, United Kingdom

Prof. Nikolay I. Zheludev
Centre for Disruptive Photonic Technologies, SPMS, TPI,
Nanyang Technological University, Singapore, 637371, Singapore

Keywords: chirality, electrogyration, optical activity, electro-optic effect, metamaterials, nanoelectromechanical systems

One of the most fascinating properties of chiral molecules is their ability to rotate the polarization of light. Since Faraday's experiments in 1845 it has been known that non-reciprocal polarization rotatory power can be induced by a magnetic field. But can reciprocal polarization rotation in chiral molecules be influenced by an electric field? In the 1960s Aizu and Zheludev introduced the phenomenon of electrogyration. While the linear (Pockels) and quadratic (Kerr) electro-optical effects describe how an external electric field changes linear birefringence and dichroism, electrogyration describes how a field changes the circular birefringence and dichroism of a medium. Electrogyration has been observed in dielectrics, semiconductors and ferroelectrics, but the effect is small. This work demonstrates a nanostructured photonic metamaterial that exhibits quadratic electrogyration – proportional to the square of the applied electric field – six orders of magnitude stronger than in any natural

medium. Giant quadratic electrogyration emerges as electrostatic forces acting against forces of elasticity change the chiral configuration of the metamaterial's nanoscale building blocks and consequently its polarization rotatory power. This observation of giant electrogyration alters the perception of the effect from that of an esoteric phenomenon into a functional part of the electro-optic toolkit with application potential.

1. Introduction

Optical activity manifests itself as circular birefringence - rotation of the polarization state of light, and circular dichroism - differential transmission of circularly polarized waves. Over 200 years have passed since the discovery of optical activity by F. Arago and it is now well-understood that the effect is linked to chirality, i.e. to structures or experiments that are different from their mirror image. In 1845, M. Faraday discovered that optical activity can be changed by an external magnetic field, but it took another 117 years until the electrical counterpart of the Faraday effect was found in ferroelectric crystals, where optical activity was changed by an external electric field.[1] At around the same time, K. Aizu and I. S. Zheludev independently described this phenomenon, naming it gyroelectric effect or electrogyration.[2,3] The Faraday effect is non-reciprocal, i.e. the optical rotation continues to grow when the wave's propagation direction is reversed. In contrast, optical activity and electrogyration are reciprocal, i.e. optical rotation is compensated upon reversal of the propagation direction. Electrogyratory polarization changes that depend linearly on electric field have been reported for crystals of various point symmetry groups,[4] and quadratic electrogyration has been observed in crystalline quartz and tellurium dioxide.[5,6]

As electrogyration is weak in natural materials, anticipation has been growing that a stronger effect might be engineered in artificial chiral metamaterials.[7] Many chiral metamaterials have been shown to exhibit optical activity exceeding that of natural materials by several orders of magnitude, but the complex geometry of these typically three-dimensional (3D)

structures makes fabrication of chiral metamaterials for the optical part of the spectrum challenging[8–15] and this has limited their realization for the optical spectral range. Indeed, most 3D-chiral metamaterials, especially those with controllable chirality, are designed for terahertz and microwave radiation.[16–20] Planar chiral patterns (e.g. flat spirals) also form 3D-chiral structures with a supporting substrate, but the resulting optical activity is typically weak.[21] Reconfigurable nanomembrane metamaterials provide an extra degree of freedom for controlling structures.[22] Actuation by electromagnetic Coulomb, Lorentz, Ampère or optical forces as well as thermal stimulation can provide dynamic control over the optical properties of reconfigurable metamaterials[16,23–32] and has enabled demonstrations of giant electro-optic, magneto-electro-optic, nonlinear optical and thermo-optic effects.

Here we report on the observation of giant electrogyration in the optical part of the spectrum. An applied electric field reversibly controls the optical activity of a photonic metamaterial of nanoscale thickness, providing a 16° range of azimuth rotation and a 9° range of ellipticity angle change for transmitted near-infrared light. This change of optical activity results from electrostatic forces (between the metamaterial and a transparent electrode) that control the metamaterial's chirality via nanoscale reconfiguration of its constituent components. The effect is quadratically dependent on electric field and a million times stronger than in naturally occurring materials. Our results also suggest the emergence of higher-order electrogyration at larger applied fields.

2. Results

2.1. Local and non-local electro-optic effects

In linear optics the constitutive equation for the electric field displacement $\boldsymbol{D}(\omega)$ induced in a medium by a light wave $\boldsymbol{E}(\omega)$ with frequency ω and wave vector $\boldsymbol{k}$ is given by

$$D_i^{(1)}(\omega) = \varepsilon_{ij}(\omega) \times E_j(\omega) + \mathrm{i}\, k_l \Gamma_{ijl}(\omega) \times E_j(\omega). \quad (1)$$

Here, the local optical properties of the medium, including absorption, refraction, linear anisotropy and dichroism, are described by the frequency-dependent symmetric second rank dielectric tensor $\varepsilon_{ij}(\omega) = \varepsilon_{ji}(\omega)$. First order nonlocal effects such as circular birefringence and dichroism are introduced by the third rank nonlocality tensor, which is antisymmetric in relation to its first two indices (i.e. $\Gamma_{ijl}(\omega) = -\Gamma_{jil}(\omega)$, as required by Onsager symmetry.[33] In a static electric field $\boldsymbol{E}(0)$ the total displacement in a medium includes power expansion terms in the static field:

$$D_i(\omega) = D_i^{(1)}(\omega) + D_i^{(2)}(\omega) + D_i^{(3)}(\omega) + \cdots \quad (2)$$

where

$$D_i^{(2)}(\omega) = 2\chi_{ijl}^{(2)}(\omega, \omega, 0) \times E_j(\omega) E_l(0) + i\, k_m \Gamma_{ijlm}^{(2)}(\omega, \omega, 0) \times E_j(\omega) E_l(0) \quad (3)$$

and

$$D_i^{(3)}(\omega) = 3\chi_{ijlm}^{(3)}(\omega, \omega, 0, 0) \times E_j(\omega) E_l(0) E_m(0) + i\, k_n \Gamma_{ijlmn}^{(3)}(\omega, \omega, 0, 0) \times E_j(\omega) E_l(0) E_m(0) \quad (4)$$

Here the third rank tensor $\chi_{ijl}^{(2)}(\omega, \omega, 0)$ describes the linear electro-optic (Pockels) effect while the fourth rank tensor $\chi_{ijlm}^{(3)}(\omega, \omega, 0, 0)$ describes quadratic changes to linear birefringence and dichroism - the quadratic electro-optic (Kerr) effect. The dependence of

circular birefringence and dichroism on the first power of external static electric field is introduced by the fourth rank tensor $\Gamma^{(2)}_{ijlm}\ (\omega, \omega, 0)$, while quadratic terms in the dependence are introduced by the fifth rank tensor $\Gamma^{(3)}_{ijlmn}\ (\omega, \omega, 0, 0)$.

It should be noted that changes to linear and circular birefringence and dichroism that are quadratic in electric field can also be induced by an intense light beam itself and are described by a similar constitutive equation

$$D_i^{(3)}(\omega) = 3\chi^{(3)}_{ijlm}\ (\omega, \omega, \omega, -\omega\ ) \times E_j\ (\omega) E_l\ (\omega) E^*_m(\omega) + i\ k_n \Gamma^{(3)}_{ijlmn}\ (\omega, \omega, \omega, -\omega) \times E_j\ (\omega) E_l\ (\omega) E^*_m(\omega) \quad (5)$$

where the tensor $\chi^{(3)}_{ijlm}\ (\omega, \omega, \omega, -\omega\ )$ describes the quadratic Stark effect and the tensor $\Gamma^{(3)}_{ijlmn}\ (\omega, \omega, \omega, -\omega)$ describes the phenomenon of nonlinear optical activity.

Circular birefringence gives rise to rotation of the polarization state of light where the angle of rotation $\Delta\varphi$ of light propagating along the *z* direction with a static electric field applied along the *z* direction is proportional to the thickness of the sample *L:*

$$\Delta\varphi = \frac{\omega^2}{2c^2}\ Re\left\{\Gamma_{xyz}(\omega) + \Gamma^{(2)}_{xyzz} E_z(0) + \Gamma^{(3)}_{xyzzz}\ E_z\ (0) E_z(0)\right\} L \quad (6)$$

Earlier sources introduce an expansion of the gyration tensor in the static electric field[4]

$$g_{ij} = g^{(0)}_{ij} + \gamma_{ijl} E_l + \beta_{ijlm}\ E_l E_m + \cdots \quad (7)$$

where in relation to the constitutive equations of the medium, $g_{ij}^{(0)} = k_l \Gamma_{ijl}(\omega)$, $\gamma_{ijl} = k_m \Gamma_{ijlm}^{(2)}(\omega, \omega, 0)$, and $\beta_{ijlm} = k_n \Gamma_{ijlmn}^{(3)}(\omega, \omega, 0,0)$. In this work, we engineer a metamaterial where the latter term of quadratic electrogyration is exceptionally large.

2.2. Design of electrogyratory metamaterial

The metamaterial comprises a periodic array of patterned nanowires manufactured on a free-standing 100-nm-thick silicon nitride membrane coated with 50 nm of gold (see Methods). Nanowires with length 37 μm and width w = 500 nm, separated by gaps of d = 170 nm, were chosen to facilitate nanowire displacement (length), while preventing nanowires from touching (gaps) and enabling a non-diffracting metamaterial structure (width). Each nanowire is perforated with alternating small and large semicircular notches with radii $R_{1,2}$ = 120, 260 nm, as illustrated in **Figure 1**c and Figure 1d. The structure has periodic unit cell dimensions $P_{x,y}$ = 1340, 1370 nm chosen to avoid diffraction at experimental wavelengths above 1370 nm. Size and position of the notches on neighboring beams are chosen to form a simplified planar (2D) spiral-like hole, which can be deformed into a 3D helix-like geometry by their mutual out-of-plane displacement. To facilitate such movement, the ends of the beams - their connection points to the surrounding (unstructured) membrane - are patterned to endow neighboring beams with alternating mechanical and electrical properties: Mechanical flexibility is enhanced [inhibited] by narrowing [widening] the beam towards the ends and by extending [limiting the extent] of the notch pattern along the beam, in the y-direction; electrical isolation of every other beam is achieved by cutting a trench through the gold layer only at either end, close to the anchor points (see detail of the gold layer at top-right and bottom-left of the scanning electron microscope [SEM] image in Figure 1b).

The metamaterial is suspended above a grounded transparent indium tin oxide (ITO) back-plane at a distance of about 4 μm, as shown in Figure 1a, such that the application of a bias

voltage between the gold and ITO electrode layers leads to charge accumulation in the metamaterial, enabling electrostatic reconfiguration of its structure:[34,35] Electrically-connected beams deform (bend towards the back-plane) under the action of the applied electrostatic force, to a point where this force is balanced by the elastic restoring force generated within the beam. Electrically isolated beams do not accumulate charge, are consequently not subject to an electrostatic force, and therefore do not move. An applied voltage thus controls the metamaterial's chirality and optical activity by controlling the relative (*z* direction) displacement of the beams that make up the metamaterial structure.

The metamaterial is achiral when flat, with all beams in the same plane. **Figure 2**a demonstrates this by showing how a unit cell of the metamaterial in its planar (2D) state can be superimposed on its mirror image by a simple half-period translation in both the *x* and *y* directions. The same can also be understood by considering that the pairs of large and small semicircular notches on adjacent beams form flat spirals with alternating senses of twist (each unit cell contains two left- and two right-handed spirals). However, when alternate beams are mutually displaced in the *z*-direction these planar spirals are transformed into 3D helices all having the same sense of twist, i.e. such that a unit cell contains either four left- or four right-handed helices, depending upon the direction of mutual beam displacement. This is illustrated in Figure 2b and c, where superimposed red helical lines connecting the arcs of paired semicircular notches are extended to two full turns to more clearly reveal their handedness. The magnitude of applied voltage (electrostatic force) controls the magnitude of beam displacement, which is proportional to the pitch of the helices, and will therefore control the magnitude of optical activity.

2.3. Observation of electrogyration

On propagation through a chiral medium, a wave with initially linear polarization becomes elliptically polarized and its polarization azimuth rotates. **Figure 3** shows measurements of the voltage-dependent spectral dispersion of these polarization changes for transmission through the metamaterial of normally incident light polarized perpendicular to the beams of the structure. In the absence of an applied field (i.e. at 0 V bias) the metamaterial exhibits moderate azimuth rotation $\Delta\varphi$ [panel (a)] and ellipticity angle change $\Delta\zeta$ [panel (b)] not exceeding 6° in either case. These are a consequence of the fact that in practice the metamaterial is not perfectly flat (and therefore achiral) in its zero-bias state: small systematic mutual displacements between neighboring beams exist in the fabricated nanostructure due to the differing strengths of the widened- and narrowed-end beam anchor points and the electrical isolation trenches (a break in the gold relieves stress between the metal and dielectric layers). With increasing applied electrical bias the polarization state of transmitted light changes at an increasing rate: relatively little change is seen between 0 and 10 V, but by 18 V azimuth rotation reaches -13.3° and +22.7° at wavelengths of 1520 nm and 1600 nm respectively, and ellipticity of -23.9° is observed at an intermediate wavelength of 1560 nm. We note that the spectral positions of both the largest positive azimuth rotation and largest negative ellipticity change blue-shift with increasing bias. When recording the measurement series of Figure 3, voltage was turned on and off at each combination of voltage and wavelength, i.e. the data correspond to 360 on/off cycles of voltage application over approximately 8 hours. To investigate the reproducibility, we repeated the measurement series of Figure 3a, involving a further 360 on/off cycles of voltage application (see Supplementary Figure S1). The repeated measurement series reproduces the data in Figure 3a with an average deviation of only 0.2° azimuth rotation, indicating that repeated cycles of voltage application do not cause any significant permanent changes. Simulations of azimuth rotation as a function

of nanowire displacement show that the magnitude of the observed effect is consistent with relative nanowire displacements of up to about 300 nm (see Supplementary Figure S2).

In general, in media with low symmetry, chirality co-exists with anisotropy. The latter manifests itself as differential refraction (birefringence) and transmission (dichroism) for orthogonal linear polarizations. As in chiral media, waves with initially linear polarization become elliptically polarized with rotated polarization azimuth on propagation through anisotropic media. It is therefore necessary to distinguish between polarization changes due to chirality and anisotropy. In contrast to those associated with optical activity, polarization changes derived from anisotropy are inherently linked to certain directions in the material coordinate frame. As such, their magnitude oscillates as a function of the incident wave's polarization azimuth. Optical activity in anisotropic media thereby corresponds to the component of polarization change that does not oscillate with incident azimuth and can be evaluated as the average polarization change over all incident azimuth orientations. So, to quantify the metamaterial's optical activity in the present case, we evaluated the transmitted beam's azimuth rotation and ellipticity for linearly polarized incident light with azimuthal angles ranging from 0-180° in 15° steps, at wavelengths of 1520 nm and 1600 nm (i.e. those of maximum observed positive and negative azimuth rotation, identified in Figure 3a).

The bias voltage dependence of metamaterial optical activity, in terms of circular birefringence and dichroism (i.e. azimuth and ellipticity angle change averaged over incident polarization azimuth) is then plotted in **Figure 4**. Again, we note here that (for the reasons discussed above) optical activity is not zero at zero bias. However, circular birefringence and dichroism at both wavelengths go to zero at 8V, indicating that the field-induced deformation of the structure at this bias setting compensates for the initial relative displacement offset between neighboring nanowires, bringing the metamaterial close to its planar achiral state. This in turn implies that the handedness of the structure changes as the applied bias crosses the 8V level. This is confirmed by changes in the sign of both circular birefringence and

circular dichroism at both measurement wavelengths. Both circular birefringence and circular dichroism exhibit a nonlinear dependence on applied bias voltage, approximated as quadratic at low voltages, but saturating as the applied bias approaches 18 V. This empirical saturation voltage is determined by the device geometry and intrinsic material properties and simulations show saturation as the mutual nanowire displacement approaches 400 nm (Supplementary Figure S2).

Numerical simulations reveal a complex metamaterial response to circularly polarized light, which is characterized by electromagnetic coupling between the nanowires and charge accumulation at their edges. Without nanowire displacement, both the structure and the modes excited by LCP and RCP are achiral with glide mirror symmetry. Upon nanowire displacement, this symmetry vanishes, the structure becomes 3D-chiral and the modes excited by LCP and RCP become distinctively different, resulting in optical activity of the nanostructure (see Supplementary Figure S4).

3. Discussion

For comparison of our metamaterial to natural materials, we estimate the magnitude of the relevant tensor components from the observed electric-field-dependent optical activity. In our experimental configuration, both the propagation direction of the incident wave and the applied electric field are oriented along z. Optical activity without application of external field would be zero for a perfectly flat structure (Figure 2a). However, a small systematic displacement of neighboring beams makes our fabricated metamaterial optically active as discussed above, i.e., $\Gamma_{xyz} \neq 0$. Application of electric field yields additional deformation of the nanomechanical metamaterial. As electrostatic forces between opposite charges are always attractive, application of positive or negative electrical bias necessarily generates the same pulling force on the metamaterial. Therefore, the voltage-dependence of both

deformation and associated optical properties must be symmetric around 0 V. It follows that a Taylor expansion of the metamaterial's optical activity in electric field E_z can only include even terms proportional to E_z^0 (optical activity), E_z^2 (quadratic electrogyration), E_z^4 … . In particular, linear electrogyration cannot occur ($\Gamma_{xyzz}^{(2)} = 0$) as it is proportional to E_z^1, but quadratic electrogyration is allowed ($\Gamma_{xyzzz}^{(3)} \neq 0$). Indeed, quadratic electrogyration can be expected considering that the attractive electrostatic forces in the similar geometry of a parallel plate capacitor depend quadratically on voltage and electric field.

Consider the measured voltage-dependence of circular birefringence at a wavelength of 1600 nm (Figure 4c). In the absence of an applied voltage, the metamaterial layer of $L \approx 150$ nm thickness rotates the polarization state of the incident wave by $\Delta\varphi_0 = -2.4°$, corresponding to a rotatory power of $-16\,000°/\mathrm{mm}$, nonlocality of $\mathrm{Re}\left(\Gamma_{xyz}\right) = \frac{2c^2\Delta\varphi_0}{\omega^2 L} = -4 \times 10^8$ rad m and gyration of $\mathrm{Re}\left(g_{xy}^{(0)}\right) = -0.2$ rad. Gyration is calculated as the product of nonlocality and wave vector, taking into account the metamaterial's refractive index of 1.4 (estimated following [36]).

Polarization rotation in the metamaterial changes by $\Delta\varphi_2$ in response to electric field $E = U/h$ generated along the propagation direction by applying bias voltage U across the $h \approx 4$ μm capacitive gap between metamaterial and ground plane. (Saturation effects emerge above 16 V, suggesting that higher-than-quadratic even-order contributions may play an increasing role in this regime.) According to the fit in Figure 4c, $\frac{\Delta\varphi_2}{E^2} \approx 1.7 \times 10^{-14}$ rad m^2 V^{-2}, and in the small-displacement limit where $L \approx 150$ nm, the corresponding nonlocality tensor component $\Gamma_{xyzzz}^{(3)} = \frac{2c^2\Delta\varphi_2}{\omega^2 L E^2} \approx 1.5 \times 10^{-20}$ rad m^3 V^{-2} is equivalent to quadratic electrogyration of $\mathrm{Re}\left(\beta_{xyzz}\right) \approx 8.2 \times 10^{-14}$ rad m^2 V^{-2}. This is a million times stronger than in natural materials known to exhibit quadratic electrogyration (e.g. quartz: 4.5×10^{-20} rad m^2 V^{-2}, tellurium dioxide: 6.6×10^{-20} rad m^2 V^{-2}).[6] Electrogyration in

natural materials as well as the metamaterial results from a perturbation of the material in response to applied electric field. However, the metamaterial is designed to achieve significant mechanical perturbations that control its chirality, resulting in a much bigger electrogyration effect.

We note that statically pre-polarized metamaterials will also exhibit linear electrogyration (and possibly higher-than-linear odd-order contributions) if the applied external electric field will compete with the internal static field. For instance, this can be achieved by a metamaterial consisting of both a nanostructured membrane and a statically charged electrode, or by inserting a pre-polarized transparent ferroelectric layer as a part of the structure.

The giant quadratic electrogyration effect reported here resembles the phenomenon of nonlinear optical activity, the dependence of the rotatory power on light's intensity. Indeed, quadratic electrogyration is described by $\Gamma^{(3)}_{ijlmn}\ (\omega, \omega, 0, -0)$ and nonlinear optical activity is described by $\Gamma^{(3)}_{ijlmn}\ (\omega, \omega, \omega, -\omega)$ (see constitutive equations above). In the electrogyration effect the square of static electric field matters, while in nonlinear optical activity it is the square of optical field that matters, i.e. light intensity. Nonlinear optical activity is also very weak in natural media,[37] while purposely designed optical metamaterials show a seven orders of magnitude stronger effect,[38] and in microwave chiral structures the effect is twelve orders of magnitude stronger.[39]

4. Conclusion

In summary, we demonstrate a metamaterial where optical activity is controlled by electric field. We observe quadratic electrogyration that is more than 6 orders of magnitude larger than has been observed in natural materials. This optical phenomenon is achieved by engineering the chiral properties of a nanomechanical metamaterial, which is actuated by

electrostatic forces. Dynamic ranges of 16° azimuth rotation and 9° ellipticity angle in a metamaterial of nanoscale thickness transform electrogyration from being an obscure effect of only academic interest into a phenomenon with potential for practical application. Metamaterial nanomechanical chirality modulators could find applications in integrated photonic chips, compact dichroic spectrometers and other nanophotonic devices.

5. Experimental Section

Metadevice fabrication: The metamaterial sample was manufactured on a 100-nm-thick 0.5×0.5 mm^2 silicon nitride membrane supported by a 200-µm-thick 5×5 mm^2 silicon frame. The back side of the membrane and frame were coated with 50 nm of gold by thermal evaporation. The metamaterial array of nanowire pairs with semicircular notches was fabricated by focused ion beam milling from the gold-coated side of the bilayer, cutting through both layers of material.

For the back-plane of the device, a 0.5-mm-thick glass substrate was coated with 50 nm of indium tin oxide (ITO) from In_2O_3/SnO_2 (90/10 wt%) alloy pellets by electron beam evaporation. A base pressure of 5×10^{-6} mbar was achieved before deposition. An oxygen pressure of 1.5×10^{-4} mbar was maintained in the chamber during deposition. The ITO layer was subsequently annealed at 280 °C for 3 hours under an oxygen atmosphere to increase conductivity and transparency - sheet resistance was subsequently evaluated in a four-point probe measurement as 60 Ω sq^{-1}. The ITO film was then spin-coated with S1813 photoresist and baked at 120°C for one minute. The final device comprises the nanostructured membrane separated by the photoresist from the ITO-coated glass substrate, which forms a capacitor configuration. A channel of ~1 mm width defined in the resist by photolithography ensures that the nanomechanical metamaterial remains free to move in the assembled device. The size

of the air gap between the metamaterial and the ITO back-plane was determined to be ~4 μm based on Fabry-Perot resonances visible in the transmission spectrum of the device, obtained using a microspectrophotometer. The gap becomes slightly smaller with increasing voltage due to deformation of the membrane and the nanowires by electrostatic forces, resulting in about 5% reduction of the gap between the effective (average) nanowire position and the back-plane at 18 V. The whole structure transmits between 12% and 58% of incident power in the 1370 - 1750 nm spectral range.

Azimuth rotation and ellipticity measurements: The beam from a supercontinuum laser source was passed through an acousto-optical tunable filter to select wavelengths in the 1360-1750 nm range (with about ±5 nm bandwidth). A polarizer and super-achromatic half-wave plate were used to set the linear polarization state incident on the metamaterial device. The beam of less than 4 mm diameter was focused onto the sample by a 10× microscope objective (Nikon MRH00101), resulting in a maximum angle of incidence onto the sample of less than 5°. Another 10× objective was used to collimate the transmitted beam and a polarimeter (Thorlabs TXP 5004) was used to quantify its polarization state (averaged over 100 repeated measurement cycles, each with a 30 ms integration time). A static bias of 0 – 18 V was applied between the metamaterial (gold layer) and the ITO back-plane using a DC power supply.

Separation of optical activity and optical anisotropy: Circular birefringence $\Delta\varphi$ is evaluated as the φ_{in}-independent (average) component of polarization azimuth rotation, where φ_{in} is the polarization azimuth of the incident linearly polarized laser beam. Circular dichroism $\Delta\zeta$ is correspondingly evaluated as the φ_{in}-independent (average) component of the ellipticity angle. A more detailed description of the method for separation of optical activity and optical anisotropy can be found in References.[8, 12, 33, 38]

Supporting Information
The data from this paper is available from the University of Southampton ePrints research repository: https://doi.org/10.5258/SOTON/D1382

Acknowledgements
This work is supported by the UK's Engineering and Physical Sciences Research Council (Grant No. EP/M009122/1), the MOE Singapore (Grant No. MOE2016-T3-1-006) and the China Scholarship Council (CSC No. 201706120205). QZ would like to acknowledge constructive discussions with Dr. Artemios Karvounis during preparations for this work.

Conflict of Interest
The authors declare no conflict of interest.

Received: ((will be filled in by the editorial staff))
Revised: ((will be filled in by the editorial staff))
Published online: ((will be filled in by the editorial staff))

References

[1] H. Futama, R. Pepinsky, *J. Phys. Soc. Jap.* **1962**, *17*, 725.

[2] K. Aizu, *Phys. Rev.* **1964**, *133*, A1584–A1588.

[3] I. S. Zheludev, *Kristallografiya* **1964**, *9*, 501. English translation: *Sov. Phys. Crystallogr.* **1965**, *9*, 418–420.

[4] I. S. Zheludev, O. G. Vlokh, *Proc. Indian Acad. Sci. Chem. Sci.* **1983**, *92*, 421–427.

[5] O. G. Vlokh, *Ukr. Fiz. Zhurn.* **1970**, *15*, 758–762.

[6] O. G. Vlokh, R. O. Vlokh, *Opt. Photon. News* **2009**, *20*, 34–39.

[7] Y. Svirko, N. I. Zheludev, M. Osipov, *Appl. Phys. Lett.* **2001**, *78*(4), 498.

[8] E. Plum, V. A. Fedotov, A. S. Schwanecke, N. I. Zheludev, Y. Chen, *Appl. Phys. Lett.* **2007**, *90*, 223113.

[9] N. Liu, H. Liu, S. Zhu, H. Giessen, *Nature Photon.* **2009**, *3*, 157.

[10] E. Plum, J. Zhou, J. Dong, V. A. Fedotov, T. Koschny, C. M. Soukoulis, N. I. Zheludev, *Phys. Rev. B* **2009**, *79*, 035407.

[11] S. Zhang, Y.-S. Park, J. Li, X. Lu, W. Zhang, X. Zhang, *Phys. Rev. Lett.* **2009**, *102*, 023901.

[12] Y. Cui, L. Kang, S. Lan, S. Rodrigues, W. Cai, *Nano Lett.* **2014**, *14*, 1021.

[13] M. Esposito, V. Tasco, F. Todisco, M. Cuscuná, A. Benedetti, D. Sanvitto, A. Passaseo, *Nature Commun.* **2015**, *6*, 6484.

[14] M. Hentschel, M. Schäferling, X. Duan, H. Giessen, H. & N. Liu, *Sci. Adv.* **2017**, *3*, e1602735.

[15] I. Fernandez-Corbaton, C. Rockstuhl, P. Ziemke, P. Gumbsch, A. Albiez, R. Schwaiger, T. Frenzel, M. Kadic, M. Wegener, *Adv. Mat.* **2019**, *31*, 1807742.

[16] T. Kan, A. Isozaki, N. Kanda, N. Nemoto, K. Konishi, H. Takahashi, M. Kuwata-Gonokami, K. Matsumoto, I. Shimoyama, *Nature Commun.* **2015**, *6*, 8422.

[17] T. Kan, A. Isozaki, N. Kanda, N. Nemoto, K. Konishi, M. Kuwata-Gonokami, K. Matsumoto, I. Shimoyama, *Appl. Phys. Lett.* **2013**, *102*, 221906.

[18] L. Cong, P. Pitchappa, N. Wang, R. Singh, *Research* **2019**, *2019*, 7084251.

[19] M. Liu, Q. Xu, X. Chen, E. Plum, H. Li, X. Zhang, C. Zhang, C. Zou, J. Han, W. Zhang, *Sci. Rep.* **2019**, *9*, 4097.

[20] W. J. Choi, G. Cheng, Z. Huang, S. Zhang, T. B. Norris, N. A. Kotov, *Nat. Mater.* **2019**, *18*(8), 820.

[21] M. Kuwata-Gonokami, N. Saito, Y. Ino, M. Kauranen, K. Jefimovs, T. Vallius, J. Turunen, Y. Svirko, *Phys. Rev. Lett.* **2005**, *95*, 227401.

[22] N. I. Zheludev, E. Plum, *Nature Nanotech.* **2016**, *11*, 16.

[23] H. Tao, A. C. Strikwerda, K. Fan, W. J. Padilla, X. Zhang, R. D. Averitt, *Phys. Rev. Lett.* **2009**, *103*, 147401.

[24] M. Lapine, D. Powell, M. Gorkunov, I. Shadrivov, R. Marqués, Y. S. Kivshar, *Appl. Phys. Lett.* **2009**, *95*, 084105.

[25] J. Y. Ou, E. Plum, L. Jiang, N. I. Zheludev, *Nano Lett.* **2011**, *11*, 2142.

[26] J. Y. Ou, E. Plum, J. Zhang., N. I. Zheludev, *Nature Nanotech.* **2013**, *8*, 252.

[27] J. Valente, J. Y. Ou, E. Plum, I. J. Youngs, N. I. Zheludev, *Nature Commun.* **2015**, *6*, 7021.

[28] J. Y. Ou, E. Plum, J. Zhang, N. I. Zheludev, *Adv. Mater.* **2016**, *28*, 729–733.

[29] M. Lapine, I. V. Shadrivov, D. A. Powell, Y. S. Kivshar, *Nature Mater.* **2012**, *11*, 30.

[30] W. Zhu, Q. Song, L. Yan, W. Zhang, P. C. Wu, L. K. Chin, H. Cai, D. P. Tsai, Z. X. Shen, T. W. Deng, S. K. Ting, Y. Gu, G. Q. Lo, D. L. Kwong, Z. C. Yang, R. Huang, A.-Q. Liu, N. I. Zheludev, *Adv. Mat.* **2015**, *27*, 4739–4743.

[31] I. M. Pryce, K. Aydin, Y. A. Kelaita, R. M. Briggs, H. A. Atwater, *Nano Lett.* **2010**, *10*, 4222.

[32] T. Shimura, T. Kinoshita, Y. Koto, N. Umeda, K. Iwami, *Appl. Phys. Lett.* **2018**, *113*, 171905.

[33] Y. P. Svirko, N. I. Zheludev, *Polarization of Light in Nonlinear Optics*, Wiley, New York, USA, **1998**.

[34] H. Zhu, F. Yi, E. Cubukcu, *Nature Photon.* **2016**, *10*, 709.

[35] P. Cencillo-Abad, J. Y. Ou, E. Plum, N. I. Zheludev, *Sci. Rep.* **2017**, *7*, 5405.

[36] D. R. Smith, S. Schultz, P. Markoš, C. M. Soukoulis, *Phys. Rev. B* **2002**, *65*, 195104.

[37] S. A. Akhamanov, B. V. Zhdanov, N. I. Zheludev, A. I. Kovrigin, V. I. Kuznetsov, *JETP Letters* **1979**, *29*(5), 264.

[38] M. Ren, E. Plum, J. Xu, N. I. Zheludev, *Nature Commun.* **2012**, *3*, 833.

[39] I. V. Shadrivov, V. A. Fedotov, D. A. Powell, Y. S. Kivshar, N. I. Zheludev, *New Journal of Physics* **2011**, *13*, 033025.

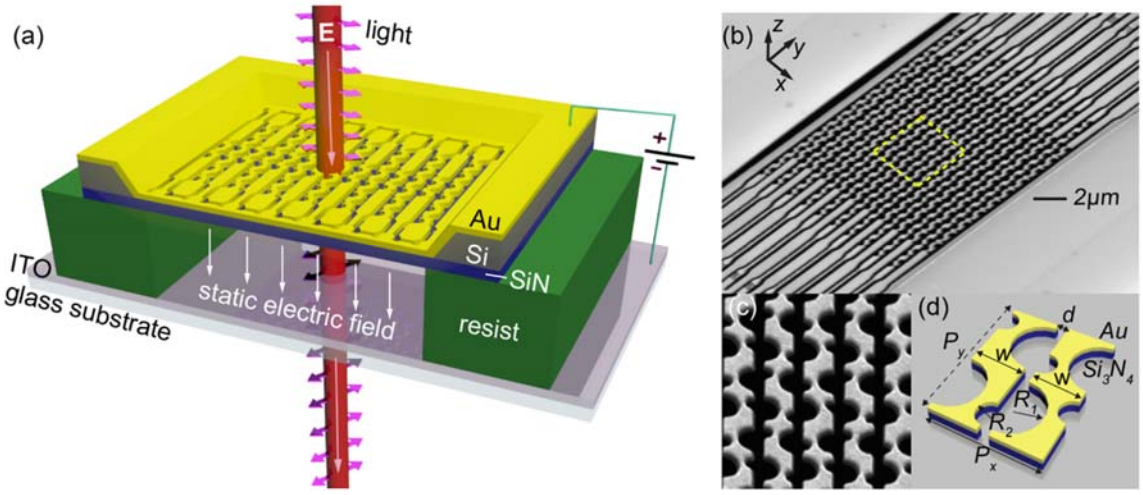

Figure 1. Electrogyratory metamaterial. (a) Artistic impression of the metamaterial, consisting of a nanostructured gold-coated silicon nitride membrane, suspended above an ITO-coated glass back-plane. Static electric field actuates the nanomechanical material, changing its chirality and optical activity. (b, c) Scanning electron microscope (SEM) images of the metamaterial. (d) Dimensional schematic of the metamaterial unit cell: $P_{x,y}$ = 1340, 1370 nm, w = 500 nm, d = 170 nm and $R_{1,2}$ =120, 260 nm.

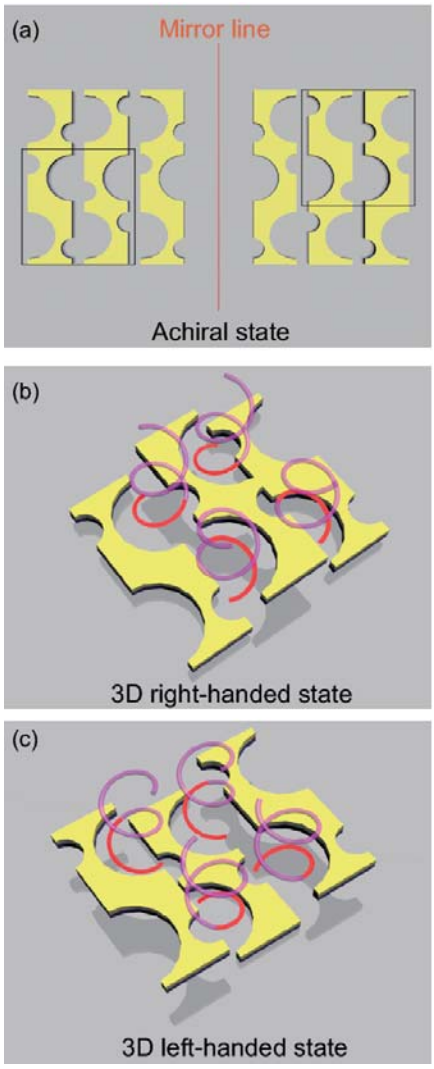

Figure 2. The origin of tunable metamaterial chirality. (a) The structure is achiral when the metamaterial beams all lie in the same plane. In this case, the metamaterial (left) and its mirror image (right) have identical unit cells (rectangular box). (b, c) With mutual out-of-plane displacement between alternate beams, either right-handed (b) or left-handed (c) chirality emerges, depending upon the direction of said displacement. In each case, the semicircular notches all form simplified helix-like geometries of the same, left or right, handedness. To aid visualization, helices are superimposed in red and extended over two full turns in purple.

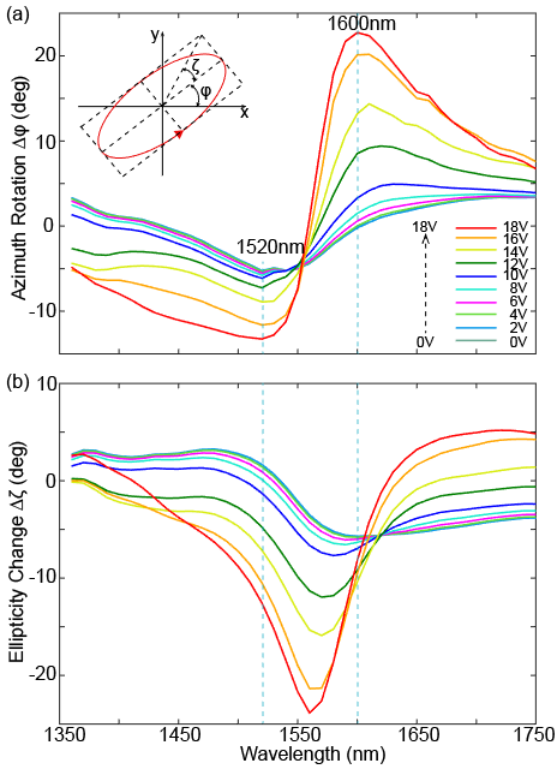

Figure 3. Control of polarization azimuth and ellipticity by electric field. Spectral dispersion of (a) azimuth rotation $\Delta\varphi$ and (b) ellipticity angle change $\Delta\zeta$ for normally incident *x*-polarized light at a selection of different applied static bias levels from 0 to 18 V. The inset defines azimuth and ellipticity angles with respect to the metamaterial coordinate frame introduced in Figure 1b.

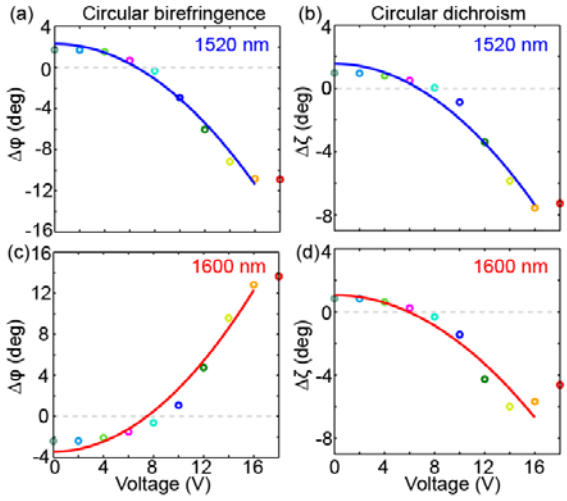

Figure 4. Giant electrogyration. Dependences on applied bias of the metamaterial's (a, c) circular birefringence in terms of average polarization azimuth rotation $\Delta\varphi$ and (b, d) circular dichroism in terms of average ellipticity angle for transmission of normally incident linearly polarized light at wavelengths of (a, b) 1520 nm and (c, d) 1600 nm. Data points are experimental results with colors corresponding to applied bias levels as in the curves of Figure 3. Lines show quadratic fits from 0 V to 16 V. (Supplementary Figure S3 shows these results in terms of Stokes parameters.)

The table of contents entry

Electrogyration, the dependence of optical activity on electric field, is a weak effect in naturally occurring materials. Co-engineering of optical and nanomechanical properties enables the realization of a photonic metamaterial structure manifesting giant electrogyration, a million times stronger than in any natural medium. Electric field actuates the nanostructure, changing its handedness and controlling both magnitude and sign of optical activity.

Qiang Zhang, Eric Plum,* Jun-Yu Ou, Hailong Pi, Junqing Li,* Kevin F. MacDonald,* and Nikolay I. Zheludev*

Electrogyration in metamaterials: Chirality and polarization rotatory power that depend on applied electric field

ToC figure (55 mm broad × 50 mm high)

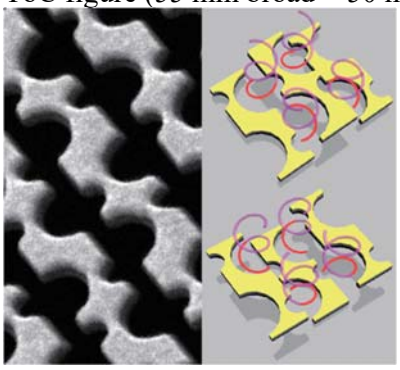

Supporting Information

Electrogyration in metamaterials: Chirality and polarization rotatory power that depend on applied electric field

Qiang Zhang, Eric Plum, Jun-Yu Ou, Hailong Pi, Junqing Li,* Kevin F. MacDonald,* and Nikolay I. Zheludev**

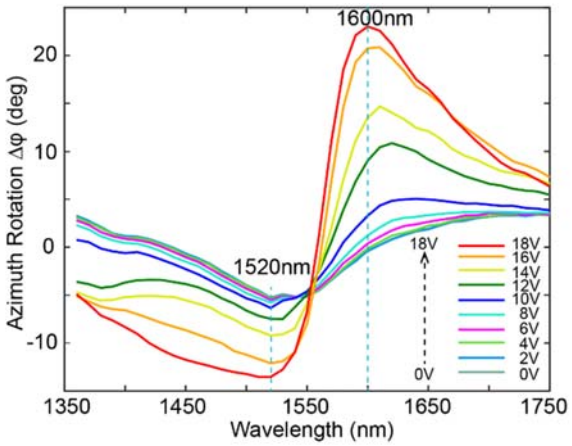

Figure S1. Repeated measurement of control of polarization azimuth by electric field. Spectral dispersion of azimuth rotation $\Delta\varphi$ for normally incident *x*-polarized light at a selection of different applied static bias levels from 0 to 18 V.

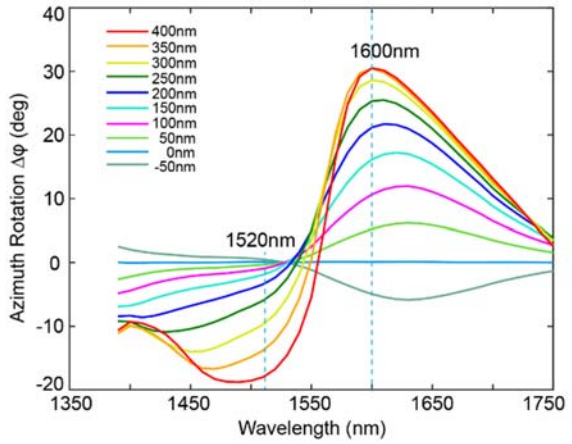

Figure S2. Simulated polarization azimuth due to relative nanowire displacement. Spectral dispersion of azimuth rotation $\Delta\varphi$ for normally incident *x*-polarized light at different relative nanowire displacements from -50 to +400 nm in 50 nm steps. Positive displacement corresponds to Figure 2b.

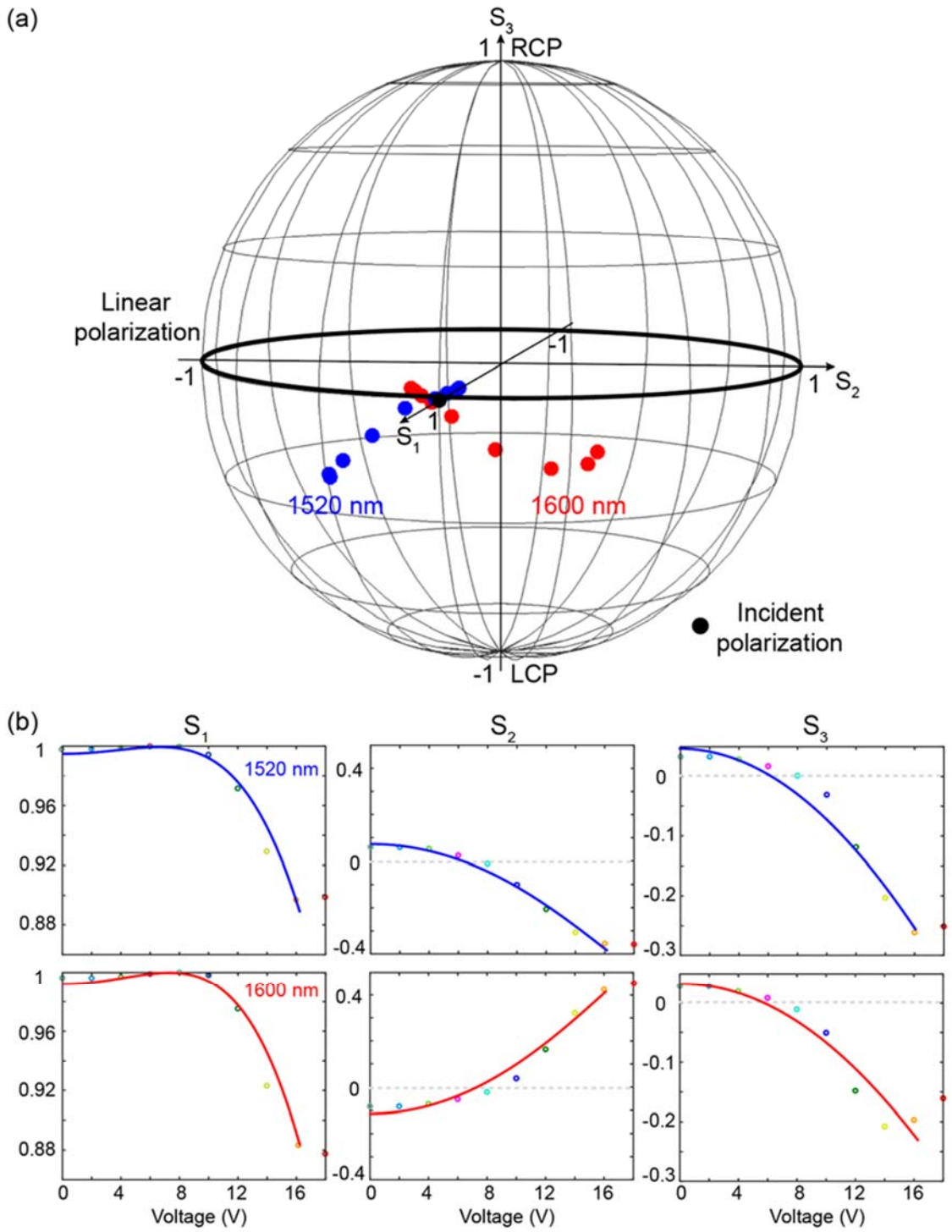

Figure S3. Giant electrogyration. The polarization changes caused by the metamaterial's optical activity at bias voltages from 0-18 V for wavelengths of 1520 nm (blue) and 1600 nm (red) in terms of Stokes parameters, presented (a) on the Poincaré sphere and (b) individually. Lines correspond to the quadratic fits of Figure 4. All Stokes vectors are normalized to S_0=1.

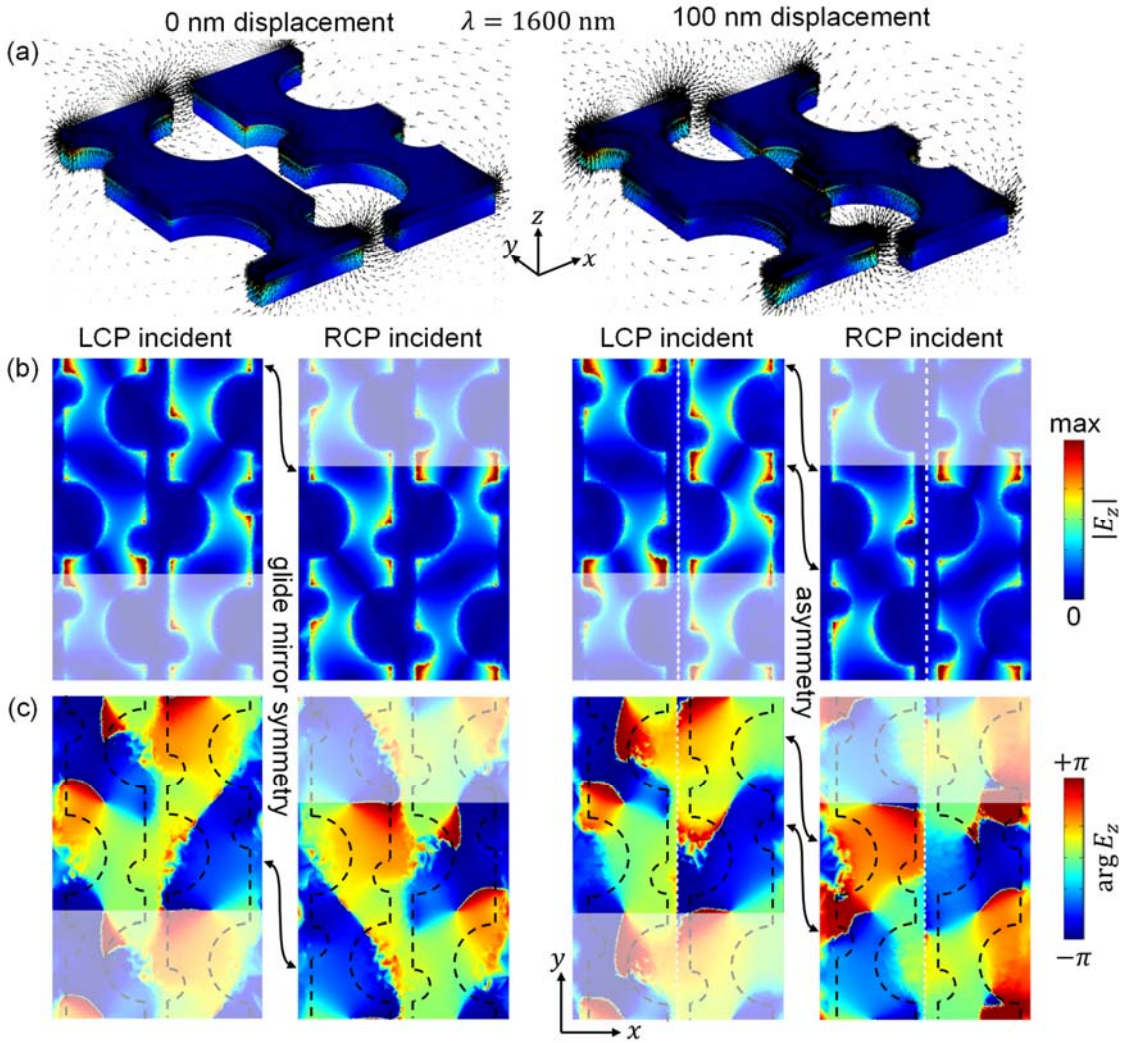

Figure S4. Metamaterial response to circularly polarized light. Results for 0 nm and 100 nm nanowire displacement and illumination of the nanostructure with normally incident light of 1600 nm wavelength according to Comsol simulations. (a) Instantaneous electric field (arrows) as well as the magnitude of the *z*-component of electric field $|E_z|$ on the nanostructure's surface for LCP illumination. (b) Magnitude and (c) phase of E_z 10 nm above the gold layer. 1.5 unit cells are shown with partial shading to visualize the glide mirror symmetry of the structure.

Metamaterial response to circularly polarized light

Simulations (Comsol) of the metamaterial response to incident light reveal substantial coupling between the nanowires (Figure S4a) and charge accumulation at their edges. Without nanowire displacement, the metamaterial is achiral and has glide mirror symmetry (left side of Figure S4). This symmetry is also present in the oscillating charge distributions that incident circularly polarized light excites in the nanostructure. LCP and RCP excite mirror-image modes in the mirror image parts of the unit cell (Figure S4b, c). Upon displacement the glide mirror symmetries of both structure and modes vanish (right side of Figure S4). The structure becomes 3D-chiral and its electromagnetic response to LCP and RCP irradiation becomes different, resulting in optical activity.